Materials Today Communications 35 (2023) 106433

Contents lists available at ScienceDirect

Materials Today Communications

journal homepage: www.elsevier.com/locate/mtcomm

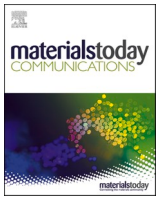

Efficient and environmentally friendly removal of azo textile dye using a low-cost adsorbent: Kinetic and reuse studies with application to textile effluent

Sabahattin Deniz

Marmara University, Faculty of Technology, Textile Engineering Dept., 34854, Maltepe, Istanbul, Türkiye

ARTICLE INFO

Keywords:
Green adsorbent
Reactive Red 21
Adsorption
MgO
Textile effluent

ABSTRACT

Recently, there has been an increasing interest in environmentally friendly methods for the removal of toxic dyes to enable sustainable textile dyeing processes. In this study, a highly efficient, non-toxic, low-cost MgO particles were prepared by sol-gel technique and utilized for the removal of Reactive Red 21 azo dye by adsorption process. The prepared MgO particles were characterized by Scanning Electron Microscopy, Fourier Transform Infrared Spectroscopy, X-Ray Diffraction, and Particle Size Analysis. The batch adsorption studies were performed for optimizing the parameters affecting adsorption. The adsorption behavior of Reactive Red 21 was accurately characterized by the Langmuir model. The adsorption process was found to be thermodynamically spontaneous at room temperatures as indicated by the negative Gibbs free energy change (ΔG) value of −30.65 kj/mol. The kinetic studies indicate that the pseudo-second-order model provides a good fit to the adsorption of Reactive Red 21. The adsorption capacity of the prepared MgO particles for Reactive Red 21 was determined to be 355 mg/g at room temperature over a wide pH range of 5–9, with a contact time of 20 min. The regeneration of dye-adsorbed MgO particles was conducted at 500 °C for 2 h. The regenerated MgO particles were then utilized for adsorbing Reactive Red 21 five times with a sufficiently high dye removal efficiency. The prepared MgO particles provided a 98 % dye removal in real textile wastewater containing Reactive Red 21 dye.

1. Introduction

Many chemical substances, including dyes and heavy metals, are released into our environment from various industrial sectors, causing many health problems [1–7]. Azo dyes have global applications in several industries, including textiles, leather, printing, food, cosmetics, and pharmaceuticals [8,9]. These dyes, which are among the most commonly used, have more than 3000 different varieties and make up over 60 % of the total amount of dyes used worldwide. Azo dyes are synthetic dyes named after the azo group (-N = N-) in their molecular structure [10]. Although they are popular in different industrial fields, they are known to have harmful effects on the environment and living organisms. Therefore, water pollution caused by textile waste, which has negative effects on the ecosystem, is a serious concern. In textile dyeing processes, since the entire dye cannot be absorbed by the fiber or fabric, wastewater from dyeing and subsequent washing contains high amounts of dye. Direct release of this wastewater into the environment leads to significant environmental issues. Amines, which are degradation products of azo dyes, create toxic effects in aquatic environments [10,11]. Due to easy contact with living organisms and rapid absorption through the skin, azo dyes pose significant health risks. In addition to allergic effects, mutagenic and carcinogenic effects are also possible [12–14]. Furthermore, wastewater containing azo dyes and their metabolites from various industries prevents penetration of sunlight into water bodies, which also reduces photosynthetic activity [15,16]. It is clear that the reactive dyes containing azo groups can result in similar environmental and public health concerns. Some reactive dyes containing azo groups, which are commonly used in the textile industry, have been found to bind to proteins or enzymes, causing abnormalities in body functions and inhibiting the function of human serum albumin [17,18].

Various physical, chemical, and biological methods are applied for the removal of dyes in textile wastewater. These include coagulation-flocculation, filtration, adsorption, ozonation, oxidation, electrolysis, and bioremediation. Each method has its own advantages and disadvantages depending on the industry where it will be applied [8,19,20]. Adsorption has emerged as a popular and effective method for removing contaminants from wastewater, owing to its high efficiency, low

E-mail address: sdeniz@marmara.edu.tr.

https://doi.org/10.1016/j.mtcomm.2023.106433
Received 20 April 2023; Received in revised form 27 May 2023; Accepted 12 June 2023
Available online 14 June 2023

operational cost, and versatility. To this end, various natural and synthetic adsorbents have been developed and applied for the removal of various pollutants, including textile dyes. Since adsorption takes place on the surface of adsorbent particles, a high surface area of an adsorbent leads to a high adsorption capacity. With this idea in mind, the synthesis and use of nanoparticles in adsorption processes have become increasingly important in recent years. For this purpose, nano fibers [21], composite nanofibers [22], metal oxides and metal oxide nano composites [23], magnetic nano composites [24] have been synthesized and successfully applied in the adsorption processes of certain dyes.

Although the adsorption capacity is inversely proportional to the particle size, the practicality of filtration in industrial-scale adsorption processes should also be considered when using nanoparticles. In such cases, adsorbents with particle sizes at the micro level, which do not pose issues in practical applications and have an acceptable adsorption capacity, can be preferred. The selection of appropriate adsorbent materials is crucial for achieving high adsorption capacity, selectivity, and stability. Additionally, the understanding of the underlying adsorption mechanisms and the optimization of process parameters are essential for the successful application of adsorption in wastewater treatment [25].

In recent years, the synthesis and use of eco-friendly adsorbents have gained significant importance. Magnesium oxide (MgO) is noteworthy as an adsorbent that is non-toxic to human health, easy to synthesize, and inexpensive [25–30].

In this study, environmentally friendly, low-cost magnesium oxide was prepared by a simple sol-gel method. MgO microparticles were utilized for the first time for removal of Reactive Red 21 azo dye and investigated its performance in real textile effluent. The synthesized adsorbent was characterized by SEM-EDS (Scanning Electron Microscopy – Energy Dispersive Spectrometry), FTIR (Fourier Transform Infrared) spectroscopy, X-Ray Diffraction (XRD) and particle size distribution analysis. The effects of parameters such as pH, contact time, and dye concentration on adsorption were investigated, and the maximum adsorption capacity was determined. In addition, adsorption isotherms and kinetic studies were conducted, and the thermodynamic evaluation of the adsorption process was performed. Regeneration and reuse studies of adsorbent were also performed.

2. Materials and methods

2.1. Materials and instrumentation

Magnesium chloride hexahydrate ($MgCl_2.6H_2O$), sodium hydroxide (NaOH), absolute ethanol (C_2H_5OH) and hydrochloric acid (HCl) were obtained from Merck. Reactive Red 21 was purchased from Remazol (as Brilliant Red BB). Distilled water was obtained from GFL 2004, for pH adjustment Henna pH meter, for mass measurements Precisa XB220 model balance were used. Hettich EBA 21 centrifuge was used for separation of solids from solutions. Shimadzu UV240 was used for absorbance measurements. SEM images and elemental composition of adsorbent were obtained by Thermo Scientific Axia ChemiSEM. FTIR spectrums were taken using Perkin Elmer Spectrum100 FTIR with Attenuated Total Reflectance (ATR) spectrophotometer. Malvern Mastersizer 3000 was used for particle size analysis. XRD analyses were performed on a Rigaku vertical diffractometer equipped with Cu Kα radiation. IKA C-MAG HS7 magnetic stirrer with ETS-D5 contact thermometer was used for preparation of adsorbent and adsorption studies. Binder oven and Lenton CAL 8000 furnace were use for thermal studies.

2.2. Preparation of magnesium oxide particles

Magnesium oxide (MgO) particles are generally prepared by sol-gel or hydrothermal technique [30–35]. In this study MgO particles sol-gel technique was carried out. 0.250 mol of $MgCl_2.6H_2O$ was dissolved with distilled water in 1 L reaction flask then kept at 70 °C for 30 min. Equivalent amount of NaOH solution was added dropwise to $MgCl_2.6H_2O$ solution with stirring vigorously at same temperature. After the addition of NaOH solution is completed, the white $Mg(OH)_2$ suspension, first was kept on the heater for 2 h and then kept at room temperature overnight (reaction 1). $Mg(OH)_2$ gel was separated by centrifuge at 5000 rpm for 5 min then washed three times with distilled water and 30 mL of absolute ethanol at once thereafter dried at 70 °C overnight. White $Mg(OH)_2$ powder was calcinated at 260 °C for 1 h, at 350 °C for 2 h and finally at 435 °C for 3 h in the air atmosphere to obtain MgO particles (reaction 2). Preparation procedure was given in Fig. S1.

$$MgCl_2 + 2NaOH \rightarrow Mg(OH)_2 + 2NaCl \quad (1)$$

$$Mg(OH)_2 \xrightarrow{\Delta} MgO + H_2O \quad (2)$$

2.3. Adsorption studies

Chemical structure and absorption spectrum of Reactive Red 21 (RR21) were given in Fig. S2. Dye adsorption studies with prepared MgO particles were conducted in batch mode with magnetic stirrer. The experiments were conducted at room temperature using 50 mL of varying concentrations of RR21 solutions and different quantities of adsorbent. The parameters affecting adsorption such as pH, dye concentration, and contact time were optimized. Dilute HCl and NaOH solutions were used for pH adjustments. In all experiments, the adsorbent and the solution were separated by centrifuging at 4000 rpm for 5 min, and the absorbances of the supernatant were measured with a UV-Vis spectrophotometer at $\lambda = 510$ nm.

Adsorption isotherm experiments were conducted at ambient temperature with dye solutions of various concentrations for a duration of 70 min. Adsorption process thermodynamics was evaluated by calculating Gibbs Free Energy change. Adsorption capacity of prepared MgO particles (q_e, mg/g) for RR21 was determined by the Eq. (3); where C_0 and C_e (mg/L) are initial and equilibrium dye concentration respectively, V (mL) is the volume of dye solution and m (g) mass of adsorbent

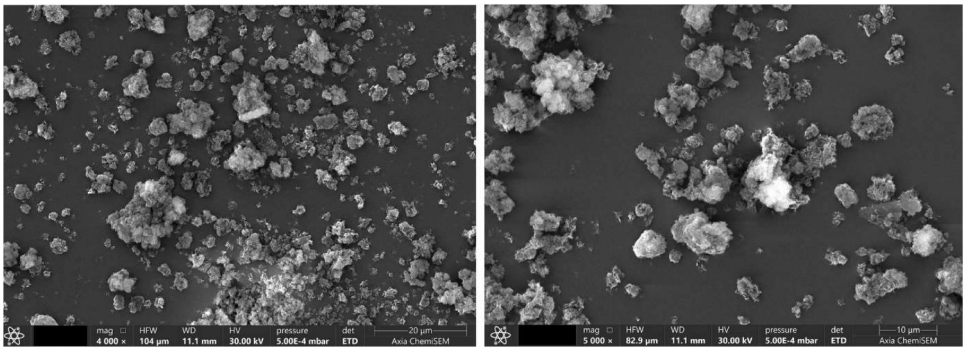

Fig. 1. SEM images of MgO particles.

Table 1
Elementel analysis result of MgO particles.

Element	Atomic %	Weight %
C	6.1	3.9
O	57.1	48.5
Mg	36.4	47.0
Si	0.3	0.4
Cl	0.1	0.2

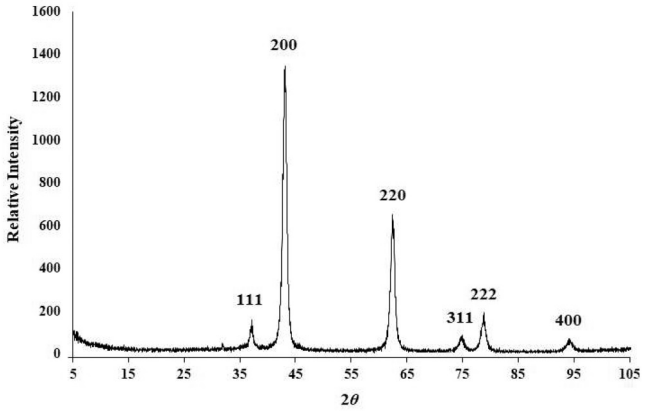

Fig. 2. XRD pattern of prepared MgO particles.

(MgO).

$$q_e = \frac{V.(C_o - C_e)}{1000.m} \quad (3)$$

3. Results and discussions

3.1. Characterization of MgO particles

MgO is an eco-friendly adsorbent, and it can be prepared different magnesium salts such as, chloride, sulfate, nitrate, acetate, or magnesium containing minerals. The use of different magnesium salts in the preparation of MgO leads to variations in the crystalline structure, particle size and therefore the specific surface area of the resulting MgO particles [36–40]. While particle sizes are generally desired to be in the nanoscale range, sometimes micro-sized particles may be more advantageous due to potential filtration or separation difficulties. In this study MgO, was prepared by sol-gel method using magnesium chloride and sodium hydroxide and obtained MgO particles were characterized by SEM-EDS, FTIR and particle size analysis.

MgO particles were prepared for SEM analysis by freeze fracturing and coated by gold approximately thickness of 300 Å. In this study, colored SEM technique was used. The colored SEM technique allows not only the definition of particle size and morphology but also an understanding of the qualitative components of the analyzed particles. The analyzed particles are colorized by a computer software based on the atoms they contain. The SEM images presented in Fig. 1. The SEM images show that the MgO particles agglomerated into needle-shaped crystals, and the agglomerated particles were approximately 10 μm in size. The colored SEM image presented in Fig. S3, and the elemental analysis results are given in Fig. S4 and in Table 1. The results indicate that the main components of the particles are Mg and O, and that they are highly pure.

To define particle size distribution and specific surface area of prepared MgO particles, particle size analysis was performed by dispersing the particles in water. According to results, the particle sizes were Dv (10) 2.22 μm, Dv(50) 8.72 μm and Dv(90) 57.9 μm in average, respectively. The specific surface area of MgO particles was determined to be

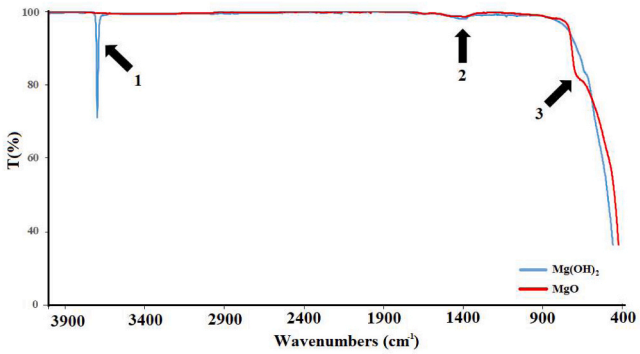

Fig. 3. FTIR spectrum of $Mg(OH)_2$ and MgO particles.

1164 m^2/kg.

XRD measurements were conducted using Cu-Kα radiation (λ = 1.5406 Å) with a step size of 0.02° (2θ), at 2-second intervals, and under operating conditions of 40 mA and 20 kV. Fig. 2 displays the diffractogram of MgO, revealing diffraction lines specific to cubic structure of MgO (Periclase, JCPDS 01-074-1225). The XRD patterns demonstrate prominent diffraction peaks of MgO at 2θ values of 37.06, 43.04, 62.26, 74.46, 78.60, 94.00 correspond to the crystal lattice planes of (111), (200), (220), (311), (222), (400) respectively. The observed diffraction patterns indicate that the adsorbent possesses a high level of crystallinity. Similar findings have been reported in previous studies [41,42].

XRD analysis of the colored particles obtained after the adsorption process was also conducted, and the results are presented in Fig. S5. According to the XRD pattern of the colored particles, it was concluded that the MgO particles hydrolyzed to $Mg(OH)_2$ [43], and this result was found to be consistent with the FTIR spectrum (Fig. 11a) of the colored particles. Additionally, XRD analyses were performed on the particles obtained through thermochemical regeneration of the colored particles, and the results are presented in Fig. S6. The XRD pattern provided in Fig. S6 indicates the reformation of MgO particles after regeneration.

MgO particle can be identify and characterize by FTIR spectroscopy [37,41–45]. FTIR spectra of $Mg(OH)_2$ and MgO obtained while synthesizing MgO were taken in the range of 4000–400 cm^{-1} wavenumbers and are given in Fig. 3. The sharp peak at 3700 cm^{-1} shows the OH band in $Mg(OH)_2$ obtained in the first step of the reaction. This peak disappeared in the spectrum of MgO as expected. $Mg(OH)_2$ and CO_2 adsorbed on the MgO surface cause the formation of carbonate species on the surface, which is observed in the spectrum as a weak peak at 1400 cm^{-1}. The shoulder at 695 cm^{-1} is due to Mg-O stretching vibration [37,44,46–48].

3.2. pH point of zero charge

The charge of the adsorbent surface is an important parameter for the types of species to be adsorbed. The surface charge of an adsorbent is dependent on the acidity of the solution. The surface charge can be predicted by the pH point of zero charge (pH_{PZC}) value of adsorbent. If the pH < pH_{PZC} then the surface of adsorbent will be positively charged if pH < pH_{PZC} than it will be negatively charged. When pH=pH_{PZC}, the net surface charge is zero [49–52]. To determine pH_{PZC} value of prepared MgO particles, 0.1 M NaCl solutions have been prepared in the range of pH 2 – 12. 0.1 g of MgO was added to 25 mL of NaCl solutions at each pH value. The mixture was stirred at constant stirring rates for 24 h, and then the final pH values were measured and the variation between the ΔpH and initial pH was plotted, and the pH_{PZC} value was found to be 10.6 (Fig S7). According to the pH_{PZC} value, it is understood that the high adsorption capacity within a wide pH range up to pH 9 is due to the positively charged surface of the adsorbent. On the other hand, it is observed that the adsorption capacity of RR21, which is an

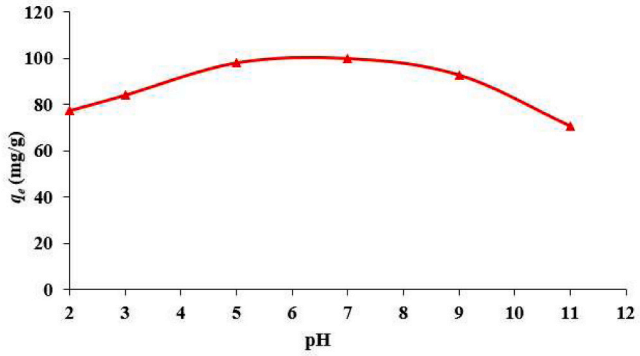

Fig. 4. Effect of initial pH on adsorption of RR21.

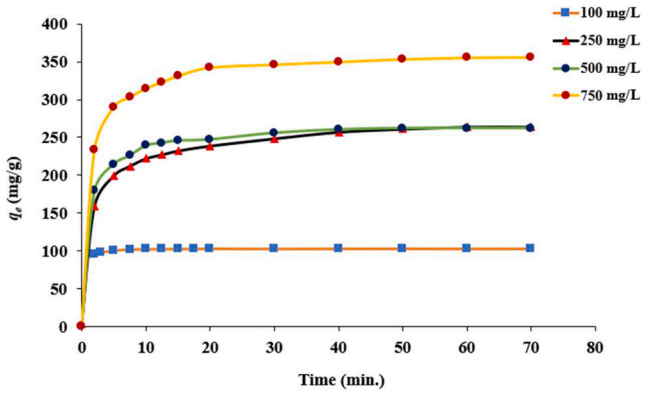

Fig. 5. Effect of contact time for the adsorption of RR21 by MgO particles.

anionic dye, decreases after pH 10, and this decrease is attributed to the adsorbent surface becoming negatively charged.

3.3. Effect of initial pH on adsorption efficiency

The effect of pH on the adsorption efficiency of RR21 on MgO particles was investigated using in the range of 2–11 initial pH with 0.05 g/50 mL adsorbent dose. Since magnesium oxide has a basic character, the initial pH of RR21 solutions becomes basic shortly after even if the initial pH is acidic. In acidic conditions, some magnesium oxide undergoes hydrolysis and is converted to $Mg(OH)_2$, which explains why the final pH is basic and why the particles do not dissolve. Nonetheless, this does not result in significant losses in the adsorption capacity. However, as the solution becomes more acidic (below pH 5), $-OSO_3^-$ groups of reactive red 21 probably protonated and become positively charged [53], leading to a decrease in the adsorption capacity. However, this does not cause significant losses in the adsorption capacity [41,54]. The dependence of adsorption capacity on pH was shown in Fig. 4. According to the Fig. 4, the maximum adsorption capacity is reached about neutral pH.

3.4. Effect of contact time on adsorption efficiency

In adsorption processes, the adsorbent and adsorbate must be stirred for a period of time until the adsorption equilibrium is established. Once the adsorption process begins, the adsorbate covers the active surface of the adsorbent, leading to a point where no further adsorption occurs. As a result, the adsorption capacity levels off over time, leading to a plateau in the adsorption capacity vs. time graphs. To determine optimum contact time of adsorption of RR21, experiments were conducted with 0.05 g/50 mL adsorbent dose in the range of 5 – 70 min at pH 7. The adsorption capacity of MgO particles remained constant after 20 min and the data shown in Fig. 5.

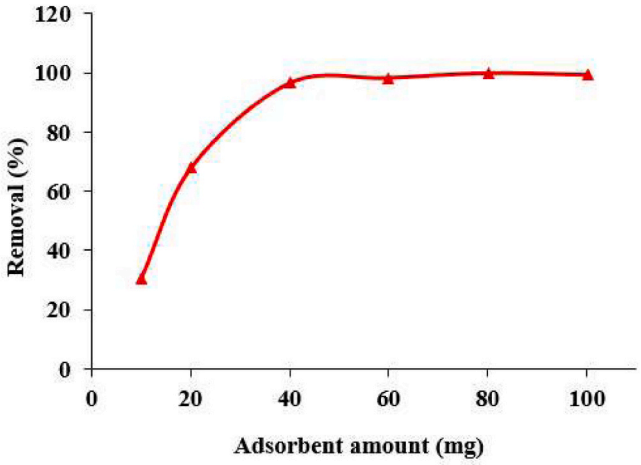

Fig. 6. Optimum MgO dose for adsorption of RR21.

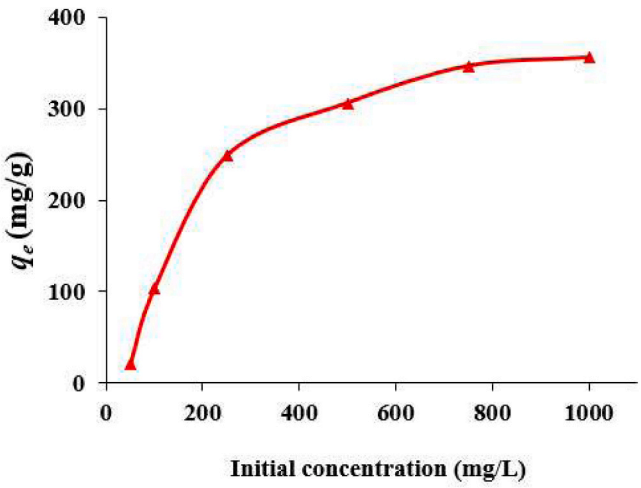

Fig. 7. The change in adsorption capacity according to initial RR21 concentration.

3.5. Adsorbent dose

The optimum amounts of adsorbent required for the adsorption of RR21 was determined by conducting experiments using various amounts of adsorbent in the range of 10–100 mg, with 50 mL of 100 mg/L dye solutions. Fig. 6 presents the data obtained from these experiments, indicating that the optimal amount of adsorbent for RR21 solution was 40 mg. The determined amount of adsorbent was then used for subsequent experiments.

3.6. Effect of RR21 concentration on adsorption

To determine adsorption capacity of prepared MgO particles for RR21, the adsorption experiments were carried out RR21 solutions in the range of 50 – 1000 mg/L at pH 7 for 20 min. Fig. 7 presents a rapid increase in adsorption capacity with increasing RR21 concentration, however after 400 mg/L a slowing down in the increase of adsorption capacity was observed and saturation in the adsorbent was reached after 750 mg/L. According to the data shown in Fig. 6, the maximum adsorption capacity of prepared MgO particles was determined as 355.33 mg/g for RR21.

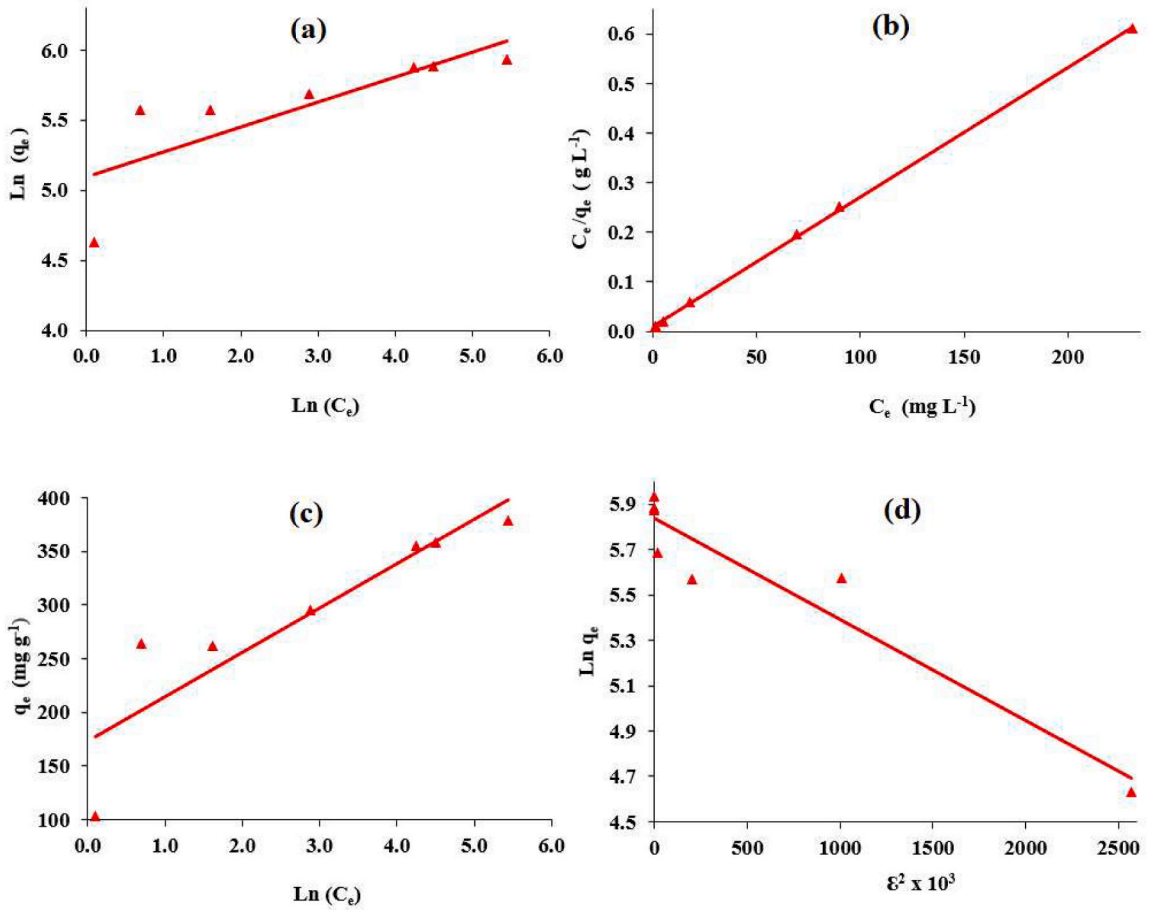

Fig. 8. Adsorption isotherm models of RR21 (a) Freundlich (b) Langmuir (c) Temkin (d) Dubinin-Radushkevich.

3.7. Adsorption isotherms

Adsorption isotherms are a valuable tool utilized for investigating the interactions between adsorbents and adsorbates. They provide essential insights regarding the nature of these interactions, the maximum amount of adsorbate that can be adsorbed, and the thermodynamic properties of the system.

A common way to represent adsorption isotherms is by plotting the amount of adsorbate that has been adsorbed against the equilibrium concentration of the adsorbate in the liquid phase. The shape of the resulting curve can give important information about the interactions between the adsorbate and adsorbent.

The Eq. (4) is commonly used to express the Langmuir isotherm, which is a model frequently employed to describe adsorption on homogeneous surfaces that covered by a monolayer of adsorbate [41, 54–56].

$$\frac{C_e}{q_e} = \frac{1}{q_{\max} K_L} + \frac{C_e}{q_{\max}} \tag{4}$$

Where C_e (mg/L), q_e (mg/g) and q_{max} are the equilibrium concentration, adsorption capacity at equilibrium and maximum adsorption capacity of the adsorbate respectively, K_L is the Langmuir constant.

The Freundlich isotherm is a theoretical model used to describe adsorption on a heterogeneous surface, where the adsorbate molecules do not form a monolayer on the surface. The Eq. (5) used to express the Freundlich isotherm is as follows [57,58]:

$$\ln q_e = \ln K_f + \frac{\ln \ C_e}{n} \tag{5}$$

Where n and K_f are empirical constants.

The Temkin isotherm model (Eq. (6)) predicts a uniform binding energy as evidenced by the linear decrease in adsorption heat for all molecule and the Dubinin-Radushkevich isotherm model is based on the concept of the potential variation on a non-uniform adsorbent surface and is expressed by Eq. 7.

$$q_e = B_T(\ln C_e + \ln K_T) \tag{6}$$

$$ln q_e = ln q_{\max} - K_{DR}\varepsilon^2 \tag{7}$$

Where B_T and K_T (L/g) are Temkin and equilibrium binding constants respectively. A positive value of B_T represents an endothermic adsorption. On the other hand, K_{DR} is the Dubinin-Radushkevich constant and ε is Polanyi potential [57].

From the Dubinin-Radushkevich isotherm data, the average

Table 2
Adsorption isotherms data.

Isotherm model and Parameters			Isotherm model and Parameters		
Langmuir	q_{max} (mg/g)	384.62	Temkin	B_T	41.354
	K_L (L.mg)	0.2857		K_T (L/mg)	65.60
	R^2	0.9995		R^2	0.8061
Freundlich	1/n	0.5919	Dubinin-Radushkevich	q_{max} (mg/g)	342.17
	K_f ((mg/g)(L/mg)$^{1/n}$)	2.783		K_{DR} (mol^2/J^2)	4×10^{-7}
	R^2	0.6567		R^2	0.9145
				E (kJ/mol)	1.118

Table 3
Parameters of the kinetic model for the adsorption process of RR21 onto MgO.

	$q_{e\ (exp)}$ (mg/g)	$q_{e\ (cal)}$ (mg/g)	k_1, k_2 (1/min.)	R^2
Pseudo-first-order model	357.23	69.73	5.85×10^{-2}	0.9799
Pseudo-second-order model		357.14	2.13×10^{-3}	1.0000

adsorption energy can be calculated as follows:

$$E = \frac{1}{\sqrt{2K_{DR}}} \tag{8}$$

The adsorption process can be categorized based on the average adsorption energy (E). E values less than 8 kj/mol indicate physical adsorption, E values between 8 and 16 kj/mol indicate ion exchange, and E values between 20 and 40 kj/mol indicate chemical adsorption.

The adsorption characteristics of RR21 onto MgO particles were studied by performing adsorption isotherm experiments at room temperature and neutral pH using dye concentrations ranging from 25 to 1000 mg/L and the plots and the data were given in Fig. 8 and in Table 2.

Based on the experimental data, it was found that the adsorption behavior of RR21 can be accurately represented by the Langmuir model, with high correlation coefficient. This suggests that a single-layer chemical adsorption process occurred, indicating the presence of homogeneous adsorption sites on the adsorbent. The Dubinin-Radushkevich data also revealed positive E values, and when considering the Temkin constants (B_T), it can be concluded that the adsorption process for RR21 can be described as endothermic physical adsorption [59,60].

The Gibbs energy change (ΔG) of adsorption was calculated by Eq. (9) to evaluate the spontaneity of the adsorption process and negative value of ΔG represents that the process is spontaneous. The ΔG value for adsorption of RR21 onto MgO particles was found to be −30.65 kj/mol which indicates spontaneous adsorption at room temperatures.

$$\Delta G = -\ R \cdot T \cdot \ln K_L \tag{9}$$

Where ΔG (kj/mol) is the Gibbs free energy change, R (8.314 J/mol. K) is the constant, T is the temperature in Kelvin and K_L (L/mol) is the Langmuir constant.

3.8. Adsorption kinetics

Adsorption kinetics refers to the study of the rate at which a substance is adsorbed onto a surface. Kinetic models, such as the pseudo-first-order and pseudo-second-order models, which are given by Eqs. (10) and (11) respectively, are often used to describe the adsorption process and determine the rate constants [61].

$$\log(q_e - q_t) = \log\ q_e - \frac{t}{2.303}\ k_1 \tag{10}$$

$$\frac{t}{q_t} = \frac{1}{k_2 q_e^2} + \frac{t}{q_e} \tag{11}$$

Where k_1 and k_2 (1/min.) are the reaction constants of pseudo-first and second order models respectively and q_t (mg/g) is the adsorption capacity at particular time.

Experimental data was given in Table 3 and Fig. 9. The data show that the pseudo-second-order model is the suitable kinetic model to describe the adsorption of RR21 onto MgO particles.

3.9. Adsorption mechanism

The adsorption process occurring on the adsorbent surface can be referred to as chemical adsorption if it results from strong interactions between the adsorbate and adsorbent, or as physical adsorption if it occurs due to relatively weak interactions. The primary interactions involved in the adsorption process typically include electrostatic interactions, dipole-dipole interactions, hydrogen bonding, and ion exchange [60,61]. Proposed mechanism for adsorption of RR21 onto MgO particles was given in Fig. 10. The Reactive Red 21 dye molecule possesses -OSO_3^- groups and heteroatoms such as O and N with unshared

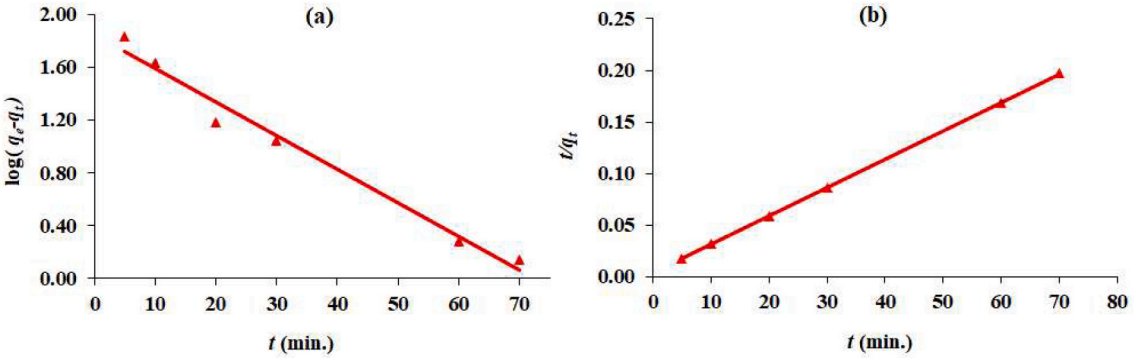

Fig. 9. Kinetic models of adsorption (a) Pseudo-first-order (b) Pseudo-second-order.

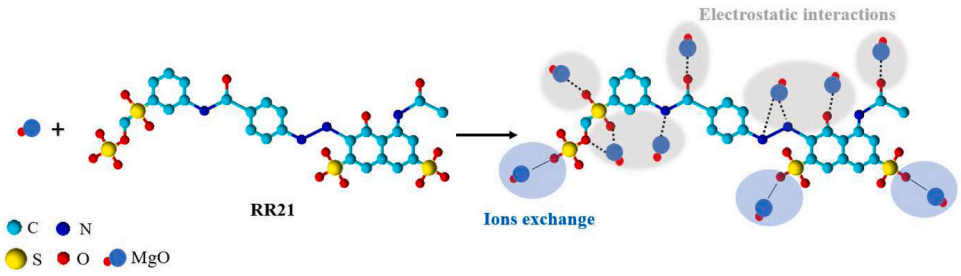

Fig. 10. Proposed adsorption mechanism of RR21 onto MgO particles.

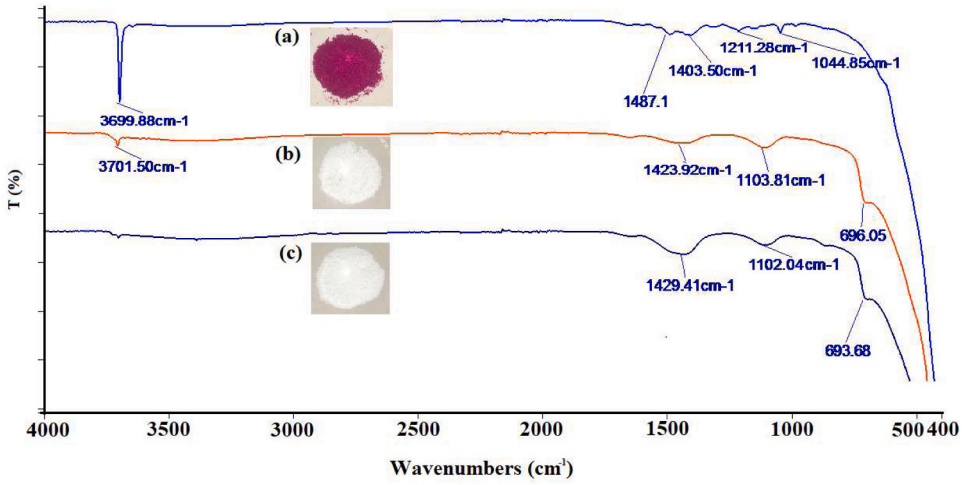

Fig. 11. Time dependent FTIR spectrums of regeneration process (a) dried colored MgO particles −0 min- (b) for 90 min (c) for 120 min.

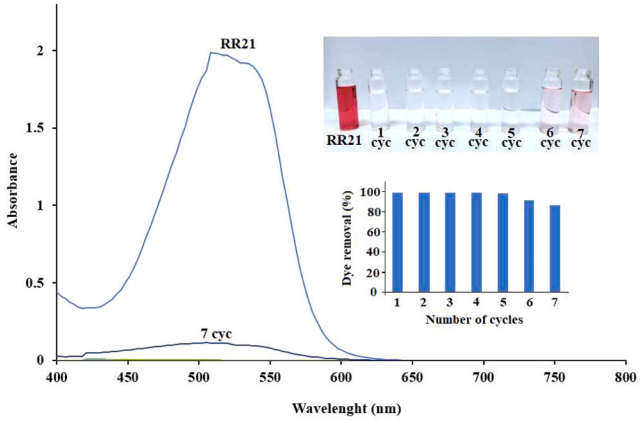

Fig. 12. Reuse of regenerated MgO particles.

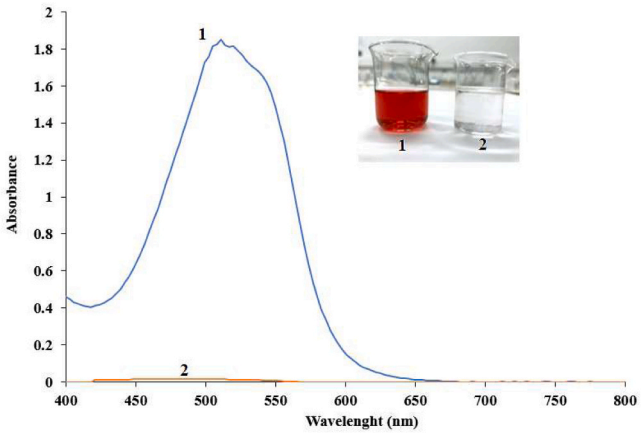

Fig. 13. Dye removal efficiency of MgO in textile effluent.

electron pairs. Therefore, in the adsorption process, it is considered to undergo ion exchange with the positive ions in MgO and also exhibit electrostatic interactions with other heteroatoms within the dye molecule.

3.10. Reuse of adsorbent

The reusability of adsorbent is the one of important issue for adsorption studies. After adsorption process, most of the time, the adsorbent it becomes a hazardous material with concentrated pollutants. MgO particles used in dye adsorption can be regenerated by thermochemical method [16,42,62].

In this study, thermochemical regeneration of MgO particles has been carried out in two steps. First, colored (dye-adsorbed) particles were dried at 70 °C for 2 h. Then dried colored MgO particles were regenerated at 500 °C in muffle furnace. Regeneration time was varied in the range of 10 – 120 min and to confirm the completion of the regeneration, FTIR spectra were taken and given in Fig. 11. From the FTIR spectra presented in Fig. 11, it was determined that a regeneration duration of 120 min would be appropriate for complete regeneration, even though white MgO particles were obtained starting from 30 min.

Although the characteristic peaks of MgO (as previously discussed above) at around 690 cm^{-1} and 1400 cm^{-1} were prominent at 90 min, the OH peak at 3700 cm^{-1} showed that there was still some $Mg(OH)_2$ present in MgO. However, after 120 min, it was concluded that $Mg(OH)_2$ had almost completely converted to MgO [37,44,46–48].

An adsorption study was conducted at neutral pH with a 100 mg/L RR21 solution for 20 min using regenerated MgO particles. The effectiveness of MgO particles, which have been regenerated many times, in removal of RR21 has been investigated, and the results are presented in Fig. 12. According to Fig. 12, it can be said that the MgO particles prepared in this study can be used five more times without a significant decrease in adsorption efficiency, provided that they are regenerated at 500 degrees for 2 h.

Although the reuse of MgO particles used for RR21 removal in aqueous environments has been successfully carried out, it is also important to evaluate the economic benefits of the regeneration process due to the low cost of the adsorbent. Additionally, proper disposal of the dye-adsorbed colored waste is also crucial. It is also important to explore different sectors where the colored particles formed after the adsorption process can be utilized. To this end, we are conducting another study on the evaluation of these waste-colored particles in textile industry.

3.11. Dye removal from real textile effluent

To evaluate how effective the prepared MgO particles in treating wastewater from textile dyeing, textile effluent containing RR21 was utilized. For this purpose, cotton fabric was dyed with reactive red 21 at a bath ratio of 1/20. Then, the fabric was washed with hot water and subsequently with detergent in a few stages. The wastewater generated during these stages of washing the fabric and the dye bath wastewater were combined to obtain the dyeing process wastewater. Properties of

Table 4
Comparing the adsorption capacity of prepared MgO particles with other adsorbents for the removal of certain reactive dyes.

Reactive Dye	Adsorbent	pH	Time	Adsorption capacity / removal efficiency	Reference
Reactive Blue 19	Corn Silk	2.0	6 h.	71.6 mg/g	[63]
Reactive Blue 19	Activated carbon magnetized with the Fe_3O_4 nanoparticles (MAC)	3.0	45 min	119.05 mg/g	[64]
Reactive Red 21	Fe–Al doped cellulose (FADC)	8.0	60 min	117.86 mg/g	[65]
Reactive Red 21	Pomelo peel biochar (PPB) and magnetic biochar composites from the pomelo peel with Fe_3O_4 (FO5-PPB)	3.0	60 min	18.59 and 26.25 mg/g	[25,66]
Reactive Yellow 86	Ag-Colemanite (COW) composite	2.0	75 min	70.82 mg/g	[67]
Reactive Red 2	Ag-Colemanite (COW) composite	2.0	75 min	66.38 mg/g	[67]
Direct Blue78	Dendrimer–titania nanocomposite	2.0	25 min	1250 mg/g	[52]
Direct Red 80	Dendrimer–titania nanocomposite	2.0	25 min	990 mg/g	[52]
Congo Red	$YMnO_3/CeO_2$/ $MgAl_2O_4$ (YCM) composite	6.8	90 min	95.20 %	[51]
Congo Red	ZnO/MgO nanocomposite	9.81	65 min	295.14 mg/g	[23]
Congo Red	$MgAl_2O_4$ nanoparticles	6.9	20 min *	89.04 mg/g	[61]
Basic Blue 41	Dithiocarbamate-functionalized graphene oxide (GO-DTC)	4.5	60 min	128.5 mg/g	[68]
Basic Red 46	Dithiocarbamate-functionalized graphene oxide (GO-DTC)	4.5	60 min	111 mg/g	[68]
Reactive Blue RS	MgO nanoparticles	3.0 – 9.0	24 h.	1000 mg/g	[27]
Reactive Blue 19	MgO nanoparticles	8	5 min	166.7 mg/g	[30]
Reactive Red 198	MgO nanoparticles	8	5 min	123.5 mg/g	[30]
Remazol Red RB-133	MgO nanoparticles	7	40 min	77.2 mg/g	[69]
Reactive Red 21	Chitosan-oxalic acid-biochar composite	5	90 min	125.1 mg/g	[70]
Reactive Red 21	*Pseudomonas aeruginosa*	8.6	96 h.	97.7 %	[71]
Acid Blue 129	Copper oxide nanoparticle loaded on activated carbon (CuO-NP-AC)	2.0	25 min	65.36 mg/g	[72]
Malachite Green	Zinc oxide nanoparticle loaded on activated carbon (ZnO-NP-AC)	7.0	15 min	322.58 mg/g	[73]
Methyl Orange	Lead oxide nanoparticles loaded activated carbon (PbO-NP-AC)	2.0	30 min	333.33 mg/g	[74]
Reactive Red 21	MgO	5.0 – 9.0	20 min	355.33 mg/g	**This study**

* Taken from Fig. 7c [58]

combined textile wastewater were given in Table S1. The effectiveness of prepared MgO particles in adsorbing RR21 in dyeing process wastewater was assessed by directly treating 50 mL of wastewater with 0.05 g adsorbent for 20 min, without any pH adjustments. According to the results presented in Fig. 13, it was observed that the prepared MgO particles provided a 98 % dye removal for RR21 in textile dyeing process wastewater.

3.12. Comparison with other studies

The removal of dye compounds from aqueous environments is of great importance due to the negative effects of textile dyes on water resources. Many studies have been carried out on this subject so far and they are still being conducted to achieve more efficient results. To evaluate the efficacy of the prepared MgO particles in adsorbing reactive dye RR21, a comparison was made with similar studies in the literature, and the results are presented in Table 4.

While there are various studies in the literature on the removal of reactive dyes from aqueous environments, there are not many studies specifically on the removal of Reactive Red 21 through adsorption method. Based on the studies conducted, Doondani et al. have achieved the highest adsorption capacity (125.1 mg/g) using a Chitosan-oxalic acid-biochar composite, while Mishra et al. have obtained a 97.7 % color removal using Pseudomonas aeruginosa bacteria as a biosorbent [67,69]. In this study, an environmentally friendly and low-cost adsorbent was prepared for the adsorption of Reactive Red 21, which has a significantly higher adsorption capacity (355.33 mg/g) and a shorter contact time (20 min) compared to the adsorbents currently available in the literature, and it was demonstrated that the adsorbent can be reused up to five times with high efficiency.

4. Conclusions

In this study, an environmentally friendly, low-cost, and highly efficient MgO particles have been prepared by sol-gel method, for adsorption of Reactive Red 21 (RR21), which an azo dye. MgO particles were characterized by FTIR, SEM-EDS, XRD and particle size analysis and it was determined that they have particle sizes of 10–50 micrometers and a specific surface area of 1164 m^2/kg. In the adsorption studies, it was determined that MgO particles have an adsorption capacity of 355.33 mg/g for Reactive Red 21 (RR21) with a contact time of 20 min at room temperature, over a wide pH range (5−9). The Langmuir model, with a high correlation coefficient, accurately describes the adsorption behavior of RR21. Positive E values were also found in the Dubinin-Radushkevich data, and by considering the Temkin constants (B_T), it can be inferred that the adsorption process of RR21 is an endothermic physical adsorption. Also, the ΔG value for adsorption process was found to be −30.65 kj/mol which indicates thermodynamically spontaneous adsorption at room temperatures. The results of the kinetic study indicate that the pseudo-second-order model provides a good fit to the experimental data and is therefore a suitable model for describing the adsorption of RR21. The dye removal efficiency of the cotton fabric dyeing wastewater treated with MgO particles was also tested, and 98 % dye removal was achieved in 20 min at room temperature without the need for any pH adjustment. The regeneration of dye-adsorbed MgO particles was conducted at 500 °C for 2 h. The regenerated MgO particles were then utilized for adsorbing RR21 five times with a sufficiently high dye removal efficiency. Additionally, the regeneration and reusability of dye-adsorbed colored waste MgO particles or their potential for alternative utilization have been discussed.

Data Availability

Data will be made available on request.

Acknowledgements

The author would like to thank Mr. Yasin Akbaş, Mr. Barış Akdeniz and Tekafos Inc. for Colored SEM and EDS analysis and the author is grateful to MSc. Özgür Çınar and Dr. Burcu Nilgün Çetiner for their incredible support that made XRD analysis possible. The author also thanks Dr. Elif Uzun Kart (Marmara University Faculty of Technology) and the Marmara University Faculty of Science Chemistry Department for allowing the use of some of their laboratory equipment.

Appendix A. Supporting information

Supplementary data associated with this article can be found in the online version at doi:10.1016/j.mtcomm.2023.106433.

References

[1] O.A. Urucu, E.K. Yetimoğlu, Ş. Dönmez, S. Deniz, Undecanol–ethanol–water ternary system-based microextraction for the detection of cadmium, J. Serb. Chem. Soc. 84 (4) (2019) 435–443, https://doi.org/10.2298/JSC180831110U.
[2] S. Deniz, G. Dartan, Y.K. Türkmenoğlu, Sistein içeren yeni bir adsorban sentezi ve sulu ortamdan Pb (II) ve Hg (II) iyonlarinin giderimi, Marmara Fen. Bilim. Derg. 30 (3) (2018) 195–200, https://doi.org/10.7240/MARUFBD.396485.
[3] O.A. Urucu, Z.Y. Gündüz, S. Deniz, E.K. Yetimoğlu, A. Aydın, A novel ligand for cloud point extraction to determine gold content in ore samples, Environ. Chem. Lett. 12 (3) (2014) 449–453, https://doi.org/10.1007/s10311-014-0471-5.
[4] M.K. Ekmekçi, M. İlhan, A.S. Başak, D. Deniz, Structural and luminescence properties of Sm^{3+} dopped TTB-Type $BaTa_2O_6$ ceramic phosphors, J. Fluoresc. 25 (2015) 1757–1762, https://doi.org/10.1007/s10895-015-1663-5.
[5] H. Birtane, O.A. Urucu, N. Yıldız, A.B. Çiğil, M.V. Kahraman, Statistical optimization and selective uptake of Au (III) from aqueous solution using carbon nanotube-cellulose based adsorbent, Mater. Today Commun. 30 (2022), 103144, https://doi.org/10.1016/j.mtcomm.2022.103144.
[6] P. Vandevivere, R.F. Bianchi, W. Verstraete, Treatment and reuse of wastewater from the textile wet-processing industry: review of emerging technologies, J. Chem. Technol. Biotech. 72 (1998) 289–302, https://doi.org/10.1002/%28SICI%291097.
[7] E.D. Aracier, E.K. Yetimoğlu, O.A. Urucu, An eco-friendly and sensitive deep eutectic solvent-based liquid-phase microextraction procedure for extraction preconcentration of Pb (II) ions, Anal. Sci. (2023) 1–7, https://doi.org/10.1007/s44211-023-00315-7.
[8] W.A. Shaikh, R.U. Islam, S. Chakraborty, Stable silver nanoparticle doped mesoporous biochar-based nanocomposite for efficient removal of toxic dyes, J. Environ. Chem. Eng. 9 (2021), 104982, https://doi.org/10.1016/j.jece.2020.104982.
[9] K. Gharanjig, M. Arami, H. Bahrami, B. Movassagh, N.M. Mahmoodi, S. Rouhani, Synthesis, spectral properties and application of novel monoazo disperse dyes derived from N-ester-1,8-naphthalimide to polyester, Dyes Pigments 76 (2008) 684–689, https://doi.org/10.1016/J.DYEPIG.2007.01.024.
[10] R. Majumdar, W.A. Shaikh, S. Chakraborty, S.R. Chowdhury, A review on microbial potential of toxic azo dyes bioremediation in aquatic system, in: S. Das, H.R. Dash. (Eds.), Microbial Biodegradation and Bioremediation, Elsevier, 2022, pp. 241–261, https://doi.org/10.1016/b978-0-323-85455-9.00018-7.
[11] P.C. Vandevivere, R. Bianchi, W. Verstraete, Review: treatment and reuse of wastewater from the textile wet-processing industry: review of emerging technologies, J. Chem. Technol. Biotechnol. 72 (1998) 289–302, https://doi.org/10.1002/(SICI)1097-4660.
[12] S. Nikfar, M. Jaberidoost, Dyes, Colorants, J.L. Coz, Encyclopedia of Toxicology, Elsevier, 2014, pp. 252–261, https://doi.org/10.1016/B978-0-12-386454-3.00602-3.
[13] F. Rafii, J.D. Hall, C. Cerniglia, Mutagenicity of azo dyes used in foods, drugs and cosmetics before and after reduction by Clostridium species from the human intestinal tract, Food Chem. Toxicol.: Int. J. Publ. Br. Ind. Biol. Res. Assoc. 35 (9) (1997) 897–901, https://doi.org/10.1016/S0278-6915(97)00060-4.
[14] W.A. Shaikh, S. Chakraborty, R.U. Islam, UV-assisted photo-catalytic degradation of anionic dye (Congo red) using biosynthesized silver nanoparticles: a green catalysis, Desalin. Water Treat. 130 (2018) 232–242, https://doi.org/10.5004/dwt.2018.23004.
[15] W.A. Shaikh, S. Chakraborty, R.U. Islam, Photocatalytic degradation of rhodamine B under UV irradiation using Shorea robusta leaf extract-mediated bio-synthesized silver nanoparticles, Int. J. Environ. Sci. Tech. 17 (2019) 2059–2072, https://doi.org/10.1007/s13762-019-02473-6.
[16] T.G. Venkatesha, Y.A. Nayaka, B. Chethana, Adsorption of Ponceau S from aqueous solution by MgO nanoparticles, Appl. Surf. Sci. 276 (2013) 620–627, https://doi.org/10.1016/j.apsusc.2013.03.143.
[17] W.Y. Li, F. Chen, S. Wang, Binding of reactive brilliant red to human serum albumin: insights into the molecular toxicity of sulfonic azo dyes, Protein Pept. Lett. 17 (5) (2010) 621–629, https://doi.org/10.2174/092986610791112756.
[18] F.O. Topaç, E. Dindar, S. Ucaroglu, H.S. Başkaya, Effect of a sulfonated azo dye and sulfanilic acid on nitrogen transformation processes in soil, J. Hazard. Mat. 170 (2–3) (2009) 1006–1013, https://doi.org/10.1016/j.jhazmat.2009.05.080.
[19] S. Liu, B. Li, P. Qi, W. Yu, J. Zhao, Y. Liu, Performance of freshly generated magnesium hydroxide (FGMH) for reactive dye removal, Colloid Interface Sci. Commun. 28 (2019) 34–40, https://doi.org/10.1016/J.COLCOM.2018.11.004.
[20] N.M. Mahmoodi, M. Bashiri, S.H. Moeen, Synthesis of nickel–zinc ferrite magnetic nanoparticle and dye degradation using photocatalytic ozonation, Mater. Res. Bull. 47 (2012) 4403–4408, https://doi.org/10.1016/j.materresbull.2012.09.036.
[21] A. Almasian, N.M. Mahmoodi, M.E. Olya, Tectomer grafted nanofiber: synthesis, characterization and dye removal ability from multicomponent system, J. Ind. Eng. Chem. 32 (2015) 85–98, https://doi.org/10.1016/J.JIEC.2015.08.002.
[22] A. Almasian, M.E. Olya, N.M. Mahmoodi, Preparation and adsorption behavior of diethylenetriamine/polyacrylonitrile composite nanofibers for a direct dye removal, Fibers Polym. 16 (2015) 1925–1934, https://doi.org/10.1007/s12221-015-4624-3.
[23] S. Wang, S.N. Tang, H. Gao, C. Yu, H. Yang, X. Yu, X.P. Chen, L. Fang, D. Li, Removal of Congo Red from Wastewater Using ZnO/MgO nanocomposites as adsorbents: equilibrium isotherm analyses, kinetics and thermodynamic studies, J. Nano Res. 77 (2023) 65–86, https://doi.org/10.4028/p-aijz91.
[24] F.S. Hosseini, S. Sadighian, H. Hosseini-Monfared, N.M. Mahmoodi, Dye removal and kinetics of adsorption by magnetic chitosan nanoparticles, Desalin. Water Treat. 57 (2016) 24378–24386, https://doi.org/10.1080/19443994.2016.1143879.
[25] G.T. Tee, X.Y. Gok, W.F. Yong, Adsorption of pollutants in wastewater via biosorbents, nanoparticles and magnetic biosorbents: a review, Environ. Res 212 (2022), 113248, https://doi.org/10.1016/j.envres.2022.113248.
[26] N. Thakur, J. Ghosh, S.K. Pandey, A. Pabbathi, J. Das, A comprehensive review on biosynthesis of magnesium oxide nanoparticles, and their antimicrobial, anticancer, antioxidant activities as well as toxicity study, Inorg. Chem. Commun. 146 (2022), 110156, https://doi.org/10.1016/j.inoche.2022.110156.
[27] S. Pourrahim, A. Salem, S. Salem, R. Tavangar, Application of solid waste of ductile cast iron industry for treatment of wastewater contaminated by reactive blue dye via appropriate nano-porous magnesium oxide, Environ. Poll. 256 (2019), 113454, https://doi.org/10.1016/j.envpol.2019.113454.
[28] A.A. Silva, A.M. Sousa, C.R. Furtado, N.M. Carvalho, Green magnesium oxide prepared by plant extracts: synthesis, properties and applications, Mater. Today Sustain. 20 (2022), 100203, https://doi.org/10.1016/j.mtsust.2022.100203.
[29] J.P. Dhal, M. Sethi, B.G. Mishra, G. Hota, MgO nanomaterials with different morphologies and their sorption capacity for removal of toxic dyes, Mater. Lett. 141 (2015) 267–271, https://doi.org/10.1016/J.MATLET.2014.10.055.
[30] G. Moussavi, M. Mahmoudi, Removal of azo and anthraquinone reactive dyes from industrial wastewaters using MgO nanoparticles, J. Hazard. Mat. 168 (2–3) (2009) 806–812, https://doi.org/10.1016/j.jhazmat.2009.02.097.
[31] B.H. Nagappa, G.T. Chandrappa, Mesoporous nanocrystalline magnesium oxide for environmental remediation, Microporous Mesoporous Mat. 106 (2007) 212–218, https://doi.org/10.1016/J.MICROMESO.2007.02.052.
[32] M.A. Aramendía, V. Borau, C. Jiménez, J.M. Marinas, J.R. Ruiz, F.J. Urbano, Influence of the preparation method on the structural and surface properties of various magnesium oxides and their catalytic activity in the Meerwein–Ponndorf–Verley reaction, Appl. Catal. A-Gen. 244 (2003) 207–215, https://doi.org/10.1016/S0926-860X%2802%2900213-2.
[33] C. Henrist, J.P. Mathieu, C. Vogels, A. Rulmont, R. Cloots, Morphological study of magnesium hydroxide nanoparticles precipitated in dilute aqueous solution, J. Cryst. Growth 249 (2003) 321–330, https://doi.org/10.1016/S0022-0248%2802%2902068-7.
[34] Q. Zhou, J. Yang, Y. Wang, Y. Wu, D. Wang, Preparation of nano-MgO/Carbon composites from sucrose-assisted synthesis for highly efficient dehydrochlorination process, Mater. Lett. 62 (2008) 1887–1889, https://doi.org/10.1016/J.MATLET.2007.10.031.
[35] M.Y. Nassar, T.Y. Mohamed, I.S. Ahmed, I. Samir, MgO nanostructure via a sol-gel combustion synthesis method using different fuels: An efficient nano-adsorbent for the removal of some anionic textile dyes, J. Mol. Liq. 225 (2017) 730–740, https://doi.org/10.1016/J.MOLLIQ.2016.10.135.
[36] E. Alvarado, L.M. Torres-Martínez, A.F. Fuentes, P. Quintana, Preparation and characterization of MgO powders obtained from different magnesium salts and the mineral dolomite, Polyhedron 19 (2000) 2345–2351, https://doi.org/10.1016/S0277-5387%2800%2900570-2.
[37] J. Hornak, Synthesis, properties, and selected technical applications of magnesium oxide nanoparticles: a review, Int. J. Mol. Sci. 22 (2021) 12752, https://doi.org/10.3390/ijms222312752.
[38] V. Karthikeyan, S. Dhanapandian, C. Manoharan, Characterization and antibacterial behavior of MgO-PEG nanoparticles synthesized via co-precipitation method, Int. Lett. Chem. Phys. and Astr. 70 (2016) 33–41, https://doi.org/10.18052/WWW.SCIPRESS.COM.
[39] Y.I. Frantina, F. Fajaroh, F. Nazriati, Yahmin Sumari, Synthesis of $MgO/CoFe_2O_4$ nanoparticles with coprecipitation method and its characterization, AIP Conf. Proc. 2330 (2021), 070003, https://doi.org/10.1063/5.0043377.
[40] R. Wahab, S.G. Ansari, M.A. Dar, Y.S. Kim, H. Shin, Synthesis of magnesium oxide nanoparticles by sol-gel process, Mater. Sci. Forum 558- 559 (2007) 983–986, https://doi.org/10.4028/www.scientific.net%2FMSF.558-559.983.
[41] Z. Camtakan, S.A. Erenturk, S. Yusan, Magnesium oxide nanoparticles: preparation, characterization, and uranium sorption properties, Environ. Prog. Sustain. Energy 31 (2012) 536–543, https://doi.org/10.1002/ep.10575.
[42] M. Mehta, M. Mukhopadhyay, R.A. Christian, Regeneration and reuse of magnesium oxide (MgO) nanocrystallites, Sep. Sci. Tech. 54 (2019) 275–281, https://doi.org/10.1080/01496395.2018.1541093.
[43] Y. Ding, G. Zhang, H. Wu, B. Hai, L. Wang, Y. Qian, Y, Nanoscale magnesium hydroxide and magnesium oxide powders: control over size, shape, and structure

via hydrothermal synthesis, Chem. Mater. 13 (2001) 435–440, https://doi.org/10.1021/CM000607E.
[44] G. Balakrishnan, R. Velavan, K.M. Batoo, E.H. Raslan, Microstructure, optical and photocatalytic properties of MgO nanoparticles, Results Phys. 16 (2020), 103013, https://doi.org/10.1016/j.rinp.2020.103013.
[45] N.C. Selvam, R.T. Kumar, L.J. Kennedy, J.J. Vijaya, Comparative study of microwave and conventional methods for the preparation and optical properties of novel MgO-micro and nano-structures, J. Alloy. Comp. 509 (2011) 9809–9815, https://doi.org/10.1016/J.JALLCOM.2011.08.032.
[46] A. Kumar, J. Kumar, On the synthesis and optical absorption studies of nano-size magnesium oxide powder, J. Phys. Chem. Solids 69 (2008) 2764–2772, https://doi.org/10.1016/J.JPCS.2008.06.143.
[47] N. Jamil, M. Mehmood, A. Lateef, R. Nazir, N. Ahsan, MgO nanoparticles for the removal of reactive dyes from wastewater, Adv. Mater.: TechConnect Briefs 1 (2015) 353–356.
[48] P. Wu, Y. Jiang, Q. Zhang, Y.F. Jia, D. Peng, W. Xu, Comparative study on arsenate removal mechanism of MgO and MgO/TiO2 composites: FTIR and XPS analysis, N. J. Chem. 40 (2016) 2878–2885, https://doi.org/10.1039/C5NJ02358K.
[49] M. Han, S. Wang, X. Chen, H. Liu, H. Gao, X. Zhao, F. Wang, H. Yang, Z. Yi, L. Fang, Spinel CuB2O4 (B = Fe, Cr, and Al) oxides for selective adsorption of Congo Red and photocatalytic removal of antibiotics, ACS Appl. Nano Mater. 5 (8) (2022) 11194–11207, https://doi.org/10.1021/acsanm.2c02349.
[50] M. Li, S. Wang, H. Gao, Z. Yin, C. Chen, H. Yang, H., L. Fang, J.A. Veerabhadrappa, Z. Yi, D. Li, Selective removal of antibiotics over MgAl2O4/C3N4/YMnO3 photocatalysts: Performance prediction and mechanism insight, J. Am. Ceram. Soc. 106 (2023) 2420–2442, https://doi.org/10.1111/jace.18946.
[51] S. Wang, M. Li, H. Gao, Z. Yin, C. Chen, H. Yang, L. Fang, J.A. Veerabhadrappa, Z. Yi, D. Li, Construction of CeO2/YMnO3 and CeO2/MgAl2O4/YMnO3 photocatalysts and adsorption of dyes and photocatalytic oxidation of antibiotics: Performance prediction, degradation pathway and mechanism insight, Appl. Surf. Sci. 608 (2023), 154977.
[52] B. Hayati, N.M. Mahmoodi, A. Maleki, Dendrimer–titania nanocomposite: synthesis and dye-removal capacity, Res. Chem. Intermed. 41 (2015) 3743–3757, https://doi.org/10.1007/s11164-013-1486-4.
[53] D. Sun, Z. Zhang, M. Wang, Y. Wu, Adsorption of reactive dyes on activated carbon developed from Enteromorpha prolifera, Am. J. Anal. Chem. 4 (2013) 17–26, https://doi.org/10.4236/ajac.2013.47A003.
[54] I. Langmuir, The adsorption of gases on plane surfaces of glass, mica and platinum, J. Am. Chem. Soc. 40 (1918) 1361–1403, https://doi.org/10.1021/JA02242A004.
[55] S. Deniz, N. Taşci, E.K. Yetimoğlu, M.V. Kahraman, New thiamine functionalized silica microparticules as a sorbent for the removal of lead, mercury and cadmium ions in aqueous media, J. Serb. Chem. Soc. 82 (2) (2017) 215–226, https://doi.org/10.2298/JSC160816098D.
[56] A. Beyler Çiğil, O. Aydın Urucu, H. Birtane, M.V. Kahraman, Cellulose/cysteine based thiol-ene UV cured adsorbent: removal of silver (I) ions from aqueous solution, Cellulose 28 (2021) 6439–6448, https://doi.org/10.1007/s10570-021-03932-5.
[57] O.A. Urucu, E.D. Aracier, E. Çakmakçi, Allylimidazole containing OSTE based photocured materials for selective and efficient removal of gold from aqueous media, Microchem. J. 146 (2019) 997–1003, https://doi.org/10.1016/J.MICROC.2019.02.041.
[58] F. Gündüz, B. Bayrak, Biosorption of malachite green from an aqueous solution using pomegranate peel: equilibrium modelling, kinetic and thermodynamic studies, J. Mol. Liq. 243 (2017) 790–798, https://doi.org/10.1016/J.MOLLIQ.2017.08.095.
[59] M.A. Ahmad, N. Ahmad, O.S. Bello, Modified durian seed as adsorbent for the removal of methyl red dye from aqueous solutions, Appl. Water Sci. 5 (2015) 407–423, https://doi.org/10.1007/s13201-014-0208-4.
[60] M. Ghasemi, S. Mashhadi, M. Asif, I. Tyagi, S. Agarwal, V. Gupta, Microwave-assisted synthesis of tetraethylenepentamine functionalized activated carbon with high adsorption capacity for malachite green dye, J. Mol. Liq. 213 (2016) 317–325, https://doi.org/10.1016/J.MOLLIQ.2015.09.048.
[61] H. Liu, S. Wang, H. Gao, H. Yang, F. Wang, X. Chen, L. Fang, S. Tang, Z. Yi, D. Li, A simple polyacrylamide gel route for the synthesis of MgAl2O4 nanoparticles with different metal sources as an efficient adsorbent: Neural network algorithm simulation, equilibrium, kinetics and thermodynamic studies, Sep. Purif. Technol. 281 (2022), 119855, https://doi.org/10.1016/j.seppur.2021.119855.
[62] T.G. Venkatesha, R. Viswanatha, Y.A. Nayaka, B. Chethana, Kinetics and thermodynamics of reactive and vat dyes adsorption on MgO nanoparticles, Chem. Eng. J. 198 (2012) 1–10, https://doi.org/10.1016/J.CEJ.2012.05.071.
[63] G.D. Değermenci, N. Değermenci, V. Ayvaoğlu, E. Durmaz, D. Çakır, E. Akan, Adsorption of reactive dyes on lignocellulosic waste; characterization, equilibrium, kinetic and thermodynamic studies, J. Clean. Prod. 225 (2019) 1220–1229, https://doi.org/10.1016/J.JCLEPRO.2019.03.260.
[64] H. Abdollahzadeh, M. Fazlzadeh, S. Afshin, H. Arfaeinia, A. Feizizadeh, Y. Poureshgh, Y. Rashtbari, Efficiency of activated carbon prepared from scrap tires magnetized by Fe3O4 nanoparticles: characterisation and its application for removal of reactive blue19 from aquatic solutions, Int. J. Env. Anal. Chem. 102 (8) (2022) 1911–1925, https://doi.org/10.1080/03067319.2020.1745199.
[65] M. Khapre, A. Shekhawat, D. Saravanan, S. Pandey, R. Jugade, Mesoporous Fe–Al-doped cellulose for the efficient removal of reactive dyes, Mater. Adv. 3 (7) (2022) 3278–3285, https://doi.org/10.1039/d2ma00146b.
[66] V.H. Nguyen, H.T. Van, V.Q. Nguyen, X.V. Dam, L.P. Hoang, L.T. Ha, Magnetic Fe_3O_4 nanoparticle biochar derived from pomelo peel for reactive red 21 adsorption from aqueous solution, J. Chem. 2020 (2020) 1–14, https://doi.org/10.1155/2020%2F3080612.
[67] M.L. Yola, T. Eren, N. Atar, S. Wang, Adsorptive and photocatalytic removal of reactive dyes by silver nanoparticle-colemanite ore waste, Chem. Eng. J. 242 (2014) 333–340, https://doi.org/10.1016/j.cej.2013.12.086.
[68] N.M. Mahmoodi, M. Ghezelbash, M. Shabanian, F. Aryanasab, M.R. Saeb, Efficient removal of cationic dyes from colored wastewaters by dithiocarbamate-functionalized graphene oxide nanosheets: From synthesis to detailed kinetics studies, J. Taiwan Inst. Chem. Eng. 81 (2017) 239–246, https://doi.org/10.1016/J.JTICE.2017.10.011.
[69] H.R. Mahmoud, S.M. Ibrahim, S.A. El-Molla, Textile dye removal from aqueous solutions using cheap MgO nanomaterials: Adsorption kinetics, isotherm studies and thermodynamics, Adv. Powder Tech. 27 (2016) 223–231, https://doi.org/10.1016/j.apt.2015.12.006.
[70] P. Doondani, V. Gomase, S. Dhandayutham, R. Jugade, Chitosan coated cotton-straw-biochar as an admirable adsorbent for reactive red dye, SSRN Electron. J. 15 (2022), 100515, https://doi.org/10.2139/ssrn.4087970.
[71] S. Mishra, P. Mohanty, A. Maiti, Bacterial mediated bio-decolourization of wastewater containing mixed reactive dyes using jack-fruit seed as co-substrate: process optimization, J. Clean. Prod. 235 (2019) 21–33, https://doi.org/10.1016/j.jclepro.2019.06.328.
[72] F. Nekouei, S. Nekouei, I. Tyagi, V. Gupta, Kinetic, thermodynamic and isotherm studies for acid blue 129 removal from liquids using copper oxide nanoparticle-modified activated carbon as a novel adsorbent, J. Mol. Liq. 201 (2015) 124–133, https://doi.org/10.1016/J.MOLLIQ.2014.09.027.
[73] M. Ghaedi, A. Ansari, M.H. Habibi, A. Asghari, Removal of malachite green from aqueous solution by zinc oxide nanoparticle loaded on activated carbon: kinetics and isotherm study, J. Ind. Eng. Chem. 20 (2014) 17–28, https://doi.org/10.1016/J.JIEC.2013.04.031.
[74] M.S. Bichave, A.Y. Kature, S.V. Koranne, R.S. Shinde, A.S. Gongle, V.P. Choudhari, N.S. Topare, S. Raut-Jadhav, S.A. Bokil, Nano-metal oxides-activated carbons for dyes removal: a review, Mater. Today.: Proc. 77 (2023) 19–30, https://doi.org/10.1016/j.matpr.2022.08.451.